Journal of Molecular Liquids 457 (2026) 129765

Contents lists available at ScienceDirect

Journal of Molecular Liquids

journal homepage: www.elsevier.com/locate/molliq

Aggregation of amyloid-like peptides in different solvents

Siwaporn Sungted [a,b], Warin Rangubpit [c], Saree Phongphanphanee [d,e], Norio Yoshida [f], Cristiano L. Dias [c,**], Jirasak Wong-Ekkabut [a,b,e,*]

[a] Department of Physics, Faculty of Science, Kasetsart University, Bangkok 10900, Thailand
[b] Computational Biomodelling Laboratory for Agricultural Science and Technology (CBLAST), Faculty of Science, Kasetsart University, Bangkok 10900, Thailand
[c] Department of Physics, New Jersey Institute of Technology, Newark, NJ 07102-1982, United States
[d] Department of Material Science, Faculty of Science, Kasetsart University, Bangkok 10900, Thailand
[e] Specialized Center of Rubber and Polymer Materials in Agriculture and Industry (RPM), Faculty of Science, Kasetsart University, Bangkok 10900, Thailand
[f] Department of Complex Systems Science, Graduate School of Informatics, Nagoya University, Nagoya 464-8601, Japan

ARTICLE INFO

Keywords:
Molecular dynamic simulations
Peptide
Aggregation
Water-octane solvent interface

ABSTRACT

The aggregation of amphipathic peptides into β-sheet rich structures is a hallmark of several neurodegenerative disorders such as Alzheimer's disease and Parkinson's disease. At the molecular level, the toxic mechanism of these peptides involves an increase in the permeation of the cellular membrane, which starts with the partition of nonpolar and polar residues at the water–lipid interface that facilitates aggregation. Here, we study this process using all-atom molecular dynamics simulations in four model peptides composed of 4 phenylalanine (F), 2 lysine (K), and 2 glutamic acid (E) under three solvent conditions. In two sequences, nonpolar and charged amino acids alternate along the chain (FKFEFKFE and FFKKFFEE), and, in the other two sequences (FFFKFEKE and FFFFKKEE), they are segregated to the N– and C–terminals. Peptides are solvated in water and octane to study aggregation in hydrophilic and hydrophobic solvents, respectively. In all simulations, peptides aggregate promptly, adopting mostly random coil conformations; except for FKFEFKFE, which spontaneously forms β-sheet conformations in water that resemble the cross-beta structures found in amyloid diseases. Aggregation takes place with a lower free energy of dimerization in octane compared to water. Simulations are also performed in a water–octane to mimic the water–lipid interface where amyloid peptides aggregate before damaging cell membranes. All peptides are spontaneously attracted to this polar–nonpolar interface which corresponds to a minimum in the free energy profile. At the interface, peptides generally exhibit low backbone interaction energies with a high content of secondary structure. The types of secondary structure formed in the system depend on the sequence pattern. In addition, the arrangement of polar and nonpolar residues modulates the free energy profile of peptide transfer from water to octane, and monomers adsorb at the interface more preferentially than the β-sheet dimer. These findings provide insights into how sequence pattern and solvent environment influence peptide aggregation, secondary structure formation, and interfacial behavior.

1. Introduction

The putative mechanism triggering Alzheimer's disease is the loss of amyloid beta (Aβ) homeostasis, which results in its gradual accumulation in the brain and the formation of low molecular weight aggregates known as oligomers. These aggregates are formed both in solution and at the water–lipid interface of cell membranes [1,2]. The latter process disrupts the integrity of the lipid membrane, contributing to Aβ toxicity. Oligomers can further aggregate into larger structures known as protofibrils, eventually forming insoluble pleated β-sheets that are the main constituents of amyloid fibrils and plaques [3]. The accumulation of these fibrils in the brain leads to inflammation, oxidative stress, and disruption of normal cellular processes, contributing to neuronal dysfunction [4]. This aggregation process is highly sensitive to the Aβ sequence wherein single point mutations can accelerate the aggregation process, reducing the onset age of Alzheimer's disease [5]. Since Alzheimer's disease arises from the aggregation of Aβ peptides into toxic oligomers that impair brain function, it is essential to elucidate the

* Corresponding author at: Department of Physics, Faculty of Science, Kasetsart University, Bangkok 10900, Thailand.
** Corresponding author.
E-mail addresses: cld@njit.edu (C.L. Dias), jirasak.w@ku.th (J. Wong-Ekkabut).

https://doi.org/10.1016/j.molliq.2026.129765
Received 24 February 2026; Received in revised form 19 June 2026; Accepted 22 June 2026
Available online 23 June 2026

mechanisms of aggregation and the effects of peptide sequence and solvent conditions.

Experimental studies on Aβ peptide mutations have demonstrated that variations in sidechain size and charge significantly impact the aggregation process. The E22G mutation is notable for significantly accelerating the aggregation of Aβ42 and leading to an increased formation of toxic oligomers, contributing to early-onset Alzheimer's disease pathology [5]. Studies on short peptide self-assembly have confirmed that different peptide sequences can lead to various structural outcomes, including the formation of distinct nanostructures or the absence of fibrils [6,7]. In addition to genetic factors, environmental conditions such as the presence of ethanol can further modulate Aβ42 behavior. A research study investigated the effect of ethanol at varying concentrations (0 to 7.2 M) on Aβ42 pentameric assemblies (Aβp) [8]. The study concluded that ethanol concentrations up to 1.4 M do not significantly destabilize Aβp. However, at the highest concentration of 7.2 M, ethanol led to the complete disassembly of Aβp into monomeric Aβ42 [8]. Environmental factors also play a significant role in peptide self-assembly; for instance, dialanine (AA) and diphenylalanine (FF) form self-assembled structures in water but not in methanol, as demonstrated by simulations and experiments [9]. In summary, experimental studies show that peptide sequence and environmental factors significantly affect aggregation and structural properties. However, experiments have a limited capacity to observe molecular interactions, demonstrating the importance of computational simulations for a more comprehensive understanding.

Computational simulations have become essential for understanding the atomic-level dynamics of aggregation. For example, a computational study on a small molecule named doxorubicin (DOX) has demonstrated how solvent interactions significantly influence aggregation, accounting for diffusion coefficients that vary across different solvents. In addition, studies of interfacial environments have revealed that DOX aggregates rapidly at these interfaces. This study showed how the magnitude of DOX–DOX compared to DOX–solvent interactions changed with the nature of the solvent [10]. For DOX, hydrogen bonding was shown to drive aggregation in water, whereas aggregation in dimethyl sulfoxide (DMSO) and other organic solvents is predominantly driven by π-stacking interactions [10]. Although computational studies offer valuable insights into molecular behavior, they encounter difficulties in studying full-length Aβ peptide aggregation due to the high computational demands and complex modeling of Aβ peptides. Consequently, several studies have focused on shorter fragments, such as the hydrophobic core $A\beta_{16–22}$, which are crucial for understanding β-sheet formation [11–14]. Short amphipathic peptides, like FKFEFKFE (labelled F1), also serve as effective models for examining peptide self-assembly mechanisms [15–17] because of their strong tendency to form β-sheets [18,19] and simpler composition than $A\beta_{16–22}$. Studies on these model peptides have helped to shed light on the effects of individual residue types in aggregation. In addition to the effects of different environments, aggregation at solvent interfaces also plays a significant role in biology. A case in point is the lipid–water interface of cell membranes that plays a crucial role in peptide aggregation, influencing the kinetics and structures formed in this process. Depending on the properties of the interface, the latter process can lead to the formation of channel-like structures that can cause membrane damage [15,20–27]. Accordingly, investigating peptide aggregation at water–hydrophobic interfaces, such as the water–octane interface, provides valuable insights into the formation of β-sheets and amyloid structures, which are crucial for understanding peptide interactions within biological membranes [28,29].

Amyloid formation is generally considered as a property of polypeptide chains [30]. Accordingly, short or designed peptides provide useful models for studying amyloid structure and aggregation [31]. Experimental studies have shown that F1 peptides self-assemble into cross-β fibrillar structures as demonstrated by AFM studies, which revealed helical ribbons with a pitch of approximately 20 nm [32,33]. Subsequent investigations have shown that their assembly behavior is sensitive to factors such as sequence length [34], hydrophobicity [18], and salt concentration [35]. In addition, F1 peptides have been widely used to investigate the role of chirality in peptide self-assembly [19,36,37]. Recently, cryo-EM studies have provided atomic-level structural insights, revealing diverse morphologies such as ribbons and nanotubes under minor variations in conditions [38]. These findings highlight the sensitivity of F1 peptide assembly to molecular details, making it an ideal model system for studying sequence- and solvent-dependent aggregation behavior. Here, we investigate how different patterns of polar and nonpolar amino acids influence peptide aggregation in different hydrophobic environments using all-atom molecular dynamics simulations. Four model peptides are used in this study, namely, FKFEFKFE (F1), FFKKFFEE (F2), FFFKFEKE (F3), and FFFFKKEE (F4). Aggregation is studied in a polar (water) and a nonpolar (octane) solvent as well as at the interface (water–octane) between these solvents. We find that peptide aggregation is energetically favorable in octane, with peptides predominantly adopting coil conformations. In contrast, aggregation in water takes place with peptides F1, F3, and F4 forming β-sheets, and peptide F2 forming α-helices. At the water–octane interface, peptides segregate polar residues to water and nonpolar residues to the octane phase. Low backbone interaction energies and a high percentage of secondary structure are observed at the interface, particularly for F1. Potential of mean force (PMF) profiles reveal that peptides in both random-coil and β-sheet configurations are preferentially located at the interface. In addition, we find that alternating sequence patterns facilitate peptide transfer from water to octane compared with segregated polar–nonpolar sequences. Transfer from water to octane is more favorable for the β-sheet dimer than for two monomers, whereas monomers exhibit a stronger preference for adsorption from water to the interface than the β-sheet dimer. These findings show the significant influence of environmental conditions and sequence patterns on peptide aggregation, providing insights into the aggregation and conformational behavior of amphipathic peptides in different solvent environments.

2. Methodology

2.1. Molecular dynamics simulations

All-atom molecular dynamics (MD) simulations are performed to investigate how the distribution of polar and nonpolar amino acids along the peptide sequence affects aggregation in different solvent conditions. Four distinct amphipathic peptides are studied: FKFEFKFE (F1), FFKKFFEE (F2), FFFKFEKE (F3), and FFFFKKEE (F4). In these sequences, nonpolar amino acids are represented by the letter F (Phenylalanine), whereas negatively and positively charged amino acids are represented by the letters E (Glutamic acid) and K (Lysine), respectively. To maintain structural integrity, the N- and C-terminals of the peptide are capped with an acetyl group ($COCH_3$) and an amino group (NH_2), respectively.

The aggregation behavior of the peptides is studied in pure water and pure octane solutions as well as at the water–octane interface. The TIP3P (Transferable Intermolecular Potential with 3 Points) model is employed for water [39], and the CHARMM36m force field is used to account for the topology of peptides and octane [40–43]. Details of the simulation setup are outlined in Table 1. The MD simulations implemented in the GROMACS 2021.5 software [44] are performed in the NPT ensemble for 1 μs. The last 100 ns are used for analysis. To assess the temporal stability of aggregation behavior, peptide–peptide hydrogen bonds were additionally analyzed using 200 ns block averages throughout the 1 μs trajectories. Sequence-dependent trends remained consistent across the simulations, with small fluctuations observed during the last stages (Fig. S1). The equations of motion are solved using the Leapfrog algorithm with an integration time step of 2 fs. Periodic boundary conditions are applied in all directions. A cut-off of 1.2 nm is used for both the Lennard-Jones and the real-space part of the electrostatic interactions. Long-range electrostatic interactions are treated using the particle-mesh

Table 1
List of simulations of all environments.

Peptides	Box size (nm^3)	No. of Peptides	Solvents	No. of Solvents	Concentration (mM)	Temperature (K)	
	9.85 × 9.85 × 9.85	10	Octane	3,221	17.37	350	310
F1	10.06 × 10.06 × 10.06	10	Water	32,210	16.30	350	310
	9.87 × 9.87 × 15.36	10	Water–Octane	32,210/1,600	11.10	350	310
	9.93 × 9.93 × 9.93	10	Octane	3,221	16.98	350	310
F2	10.06 × 10.06 × 10.06	10	Water	32,210	16.30	350	310
	9.86 × 9.86 × 15.35	10	Water–Octane	32,210/1,600	11.11	350	310
	9.89 × 9.89 × 9.89	10	Octane	3,221	17.14	350	310
F3	10.06 × 10.06 × 10.06	10	Water	32,210	16.32	350	310
	9.87 × 9.87 × 15.36	10	Water–Octane	32,210/1,600	11.11	350	310
	9.88 × 9.88 × 9.88	10	Octane	3,221	17.20	350	310
F4	10.06 × 10.06 × 10.06	10	Water	32,210	16.31	350	310
	9.86 × 9.86 × 15.34	10	Water–Octane	32,210/1,600	11.14	350	310

Ewald (PME) method [45,46], with the reciprocal-space interactions evaluated on a 0.12 nm grid with cubic interpolation of order four. All bond lengths are constrained by the P-LINCS algorithm [47]. Peptides, water, and octane are thermostated separately at 350 K using the Parrinello–Donadio–Bussi velocity rescale algorithm [48]. The Parrinello–Rahman barostat [49] is isotropically applied in the x, y, and z directions. Pressure is held constant at 1 bar using a time constant of 1 ps and a compressibility of 4.5×10^{-5} bar^{-1}. The Visual Molecular Dynamics (VMD) software [50] is used to visualize molecules. To evaluate the reproducibility of the aggregation behavior, two additional independent simulations of all peptides are performed in water, octane, and water–octane systems at 350 K for 500 ns. Furthermore, additional simulations of all peptides are performed at 310 K for 500 ns with three replicas. The aggregation behavior and secondary structure content observed at 310 K is qualitatively similar to the results observed at 350 K as shown in Figs. S2, S3, and S4.

2.2. Molecular interaction analysis

All analyses are performed using tools provided in the GROMACS software package. Clustering was defined such that peptides were considered to belong to the same cluster when the minimum distance between any atoms of the peptides was within 0.35 nm [51,52]. The coordination number is defined by the average number of solvent molecules (water or octane) surrounding a given amino acid residue within the first coordination shell. It was calculated by integrating the radial distribution function (RDF) between each residue type and the corresponding solvent from zero up to the first minimum, which defines the boundary of the first coordination shell. A hydrogen bond [53] is formed when the distance (r_{HB}) between donor and acceptor groups is < 0.35 nm and the hydrogen-donor-acceptor angle (α_{HB}) is $< 30°$. The alignment of the peptide with respect to the interface is determined by measuring the angle between two vectors: one connecting the Cα atoms of the first and last residues of each peptide, and the other being the z-axis (perpendicular to the interface). The radius of gyration (Rg) is calculated using the position of the Cα atoms, and the end-to-end distance (D_{NN}) is defined as the distance between the Cα atoms of the first and last residues of each peptide. Conformational free energy landscapes were constructed from the joint probability distribution of Rg and D_{NN} using the Boltzmann relation: $\Delta G(Rg, D_{NN}) = -k_B T \ln P(Rg, D_{NN})$, where $\Delta G(Rg, D_{NN})$ is the free energy at a given pair of Rg and D_{NN} values, $P(Rg, D_{NN})$ is the normalized probability of observing that conformation, k_B is the Boltzmann constant, and T is the system temperature. Secondary structure of peptides is determined using the Dictionary of Secondary Structure in Proteins (DSSP) tool [54]. Backbone interaction energies are calculated as the sum of electrostatic and van der Waals components for the relevant atom groups.

2.3. Solvation free energy of peptides in pure solvents

The solvation free energy was calculated using the three-dimensional reference interaction site model (3D-RISM). In the calculation, the solute conformations used were taken from the MD simulations of monomer and dimer peptides that were performed in the pure water and pure octane for 1 μs. The peptide conformations were sampled every 1 ns. For the solvents, TIP3P [39] and the CHARMM36 united-atom force field [55] were used for water and octane, respectively. The united-atom (UA) model was chosen to improve numerical stability and convergence in 3D-RISM calculations. The previous studies suggest that UA reproduces solvation free energies in reasonable agreement with experimental data [56–59]. The solvent–solvent correlation functions of the solvents were obtained by RISM with Kovalenko-Hirata closure (KH closure) [60]. The 3D-RISM equation coupled with the KH closure was solved on a grid of 128 × 128 × 128 points with a spacing of 0.5 Å. All RISM and 3D-RISM calculations were performed using the Reference Interaction Site Model Integrated Calculator (RISMiCal) package [61,62].

2.4. Potential of mean force profiles

The potential of mean force (PMF) profiles for the translocation of a single peptide and a β-sheet through the water–octane interface are calculated by umbrella sampling with the weighted histogram analysis method (WHAM) [63,64]. Simulations were conducted under the NPT ensemble at a temperature of 350 K. A harmonic restraint with a force constant of 3,000 kJ mol^{-1} nm^{-2} was applied to pull the peptide movement across the interface from water to octane phases along the z-axis. The distance between the center of mass (COM) of the peptide and the center of the octane phase was varied systematically from 0 to 5 nm with the increments of 0.1 nm. Each window was simulated for 50 ns, and the trajectories from the last 5 ns were extracted for free energy calculations. Statistical errors in the PMF were estimated using bootstrap analysis [64]. To evaluate the stability of the dimer configuration along the reaction coordinate, the minimum inter-peptide distance was calculated for each umbrella sampling window using the last 5 ns of simulation. A configuration was defined as a dimer when the minimum distance between the two peptides was less than 0.5 nm [65,66].

3. Results and discussions

3.1. Peptide aggregation in water and octane solutions

In simulations performed in water and octane solutions, 10 peptides are initially distributed randomly in the box. As time evolves, they promptly aggregate into a single cluster as quantified by the size of the largest cluster in Fig. 1a. For all peptides, the size of the largest cluster reaches the maximum value of 10 before the end of the simulation. This takes place faster, accounting for more stable clusters (i.e., clusters with less fluctuations in their sizes), in octane (green line) compared to water (blue line). This behavior is consistently observed in the independent replicate simulations (Fig. S5). The structures of the different clusters formed in water and octane solutions at the end of the simulation are

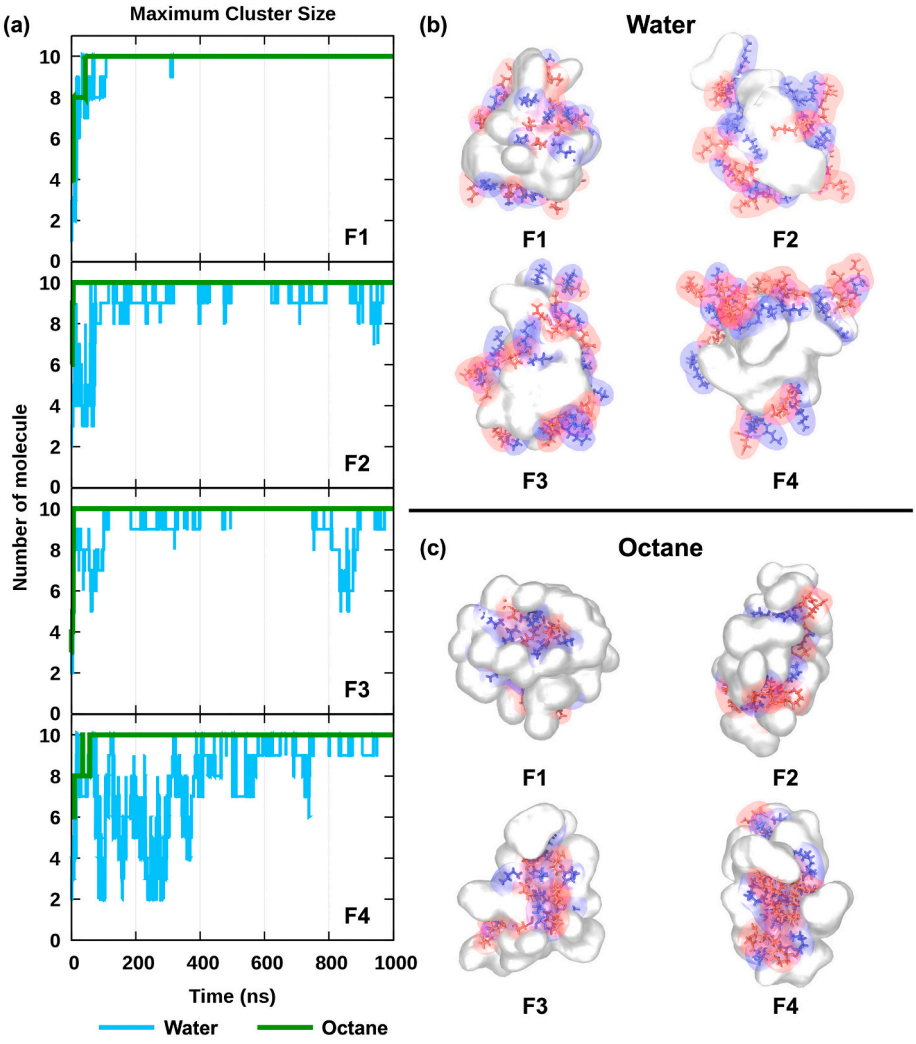

Fig. 1. Aggregation dynamics and final configurations for all peptide sequences. (a) Time evolution of the peptide count in the largest aggregate cluster with a cut-off of 0.35 nm, comparing water (blue) and octane (green) environments. Final configuration snapshots of peptide aggregates in (b) water and (c) octane, with amino acid residues colour-coded: phenylalanine (white), lysine (blue), and glutamic acid (red). (For interpretation of the references to colour in this figure legend, the reader is referred to the web version of this article.)

illustrated in Fig. 1b and 1c, respectively. Visually, charged (lysine, K, and glutamic acid, E) residues in these clusters appear more exposed to the solvent in water (panel b) than in octane (panel c). Characterization of amphiphilic molecules in water shows that they form aggregates with polar groups oriented toward the surrounding water, whereas the hydrophobic chains cluster in the inner core [67]. In contrast, clusters in panel c show a preferential exposure of nonpolar (phenylalanine, F) residues to the solvent in octane. This preferential interaction of charged residues with water and of nonpolar residues with octane is quantified in Fig. 2 by computing the coordination number of solvent molecules around lysine, glutamic acid, and phenylalanine residues in simulations performed with F1 peptides. The preferential interaction with water is indicated by a significantly larger coordination number of water molecules around lysine and glutamic acid (> 14) when compared to phenylalanine (~ 6). In octane, the coordination number of octane molecules around phenylalanine is slightly larger (~ 4.8) than around lysine and glutamic acid (< 3). Notice that these preferences are independent of the amino acid sequence, as shown in Fig. S6 for peptides F2–F4. This hydrophobic core influences the formation of secondary structures [68].

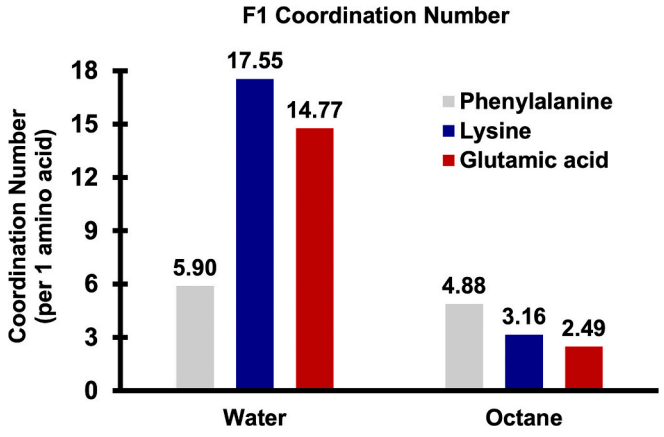

Fig. 2. Coordination number, defined as the number of solvent molecules within the first coordination shell, for each residue of the F1 peptide in pure water and pure octane. Residue types are colour-coded: gray for phenylalanine, blue for lysine, and red for glutamic acid. (For interpretation of the references to colour in this figure legend, the reader is referred to the web version of this article.)

3.2. Hydrogen bond formation

To provide insights into the different cluster structures formed during aggregation, we focus on hydrogen bond (Hbond) formation. In simulations performed with F1 peptides in water, Fig. 3a shows that initially the numbers of peptide–peptide (black line) and peptide–solvent (red line) Hbonds increase and decrease, respectively. This is consistent with a picture where peptides aggregate during the simulation and, thus, interact less with the solvent and more with each other [69,70]. Furthermore, the total number of peptide–peptide Hbonds in water is decomposed into Hbonds formed only by atoms of the same chain (intra-peptide, cyan line) and Hbonds involving atoms of two different chains (inter-peptide, magenta line). Inter-peptide Hbonds dominate over intra-peptide Hbonds for sequences F1 (Fig. 3a), F3, and F4 (Fig. S7), which could be indicative of β-sheet formation. In contrast, F2 peptides in water mainly form Hbonds within the same peptide (Fig. S7). This may be indicative of α-helical conformations when Hbonds are formed between residues i and i + 4.

Fig. 3b shows the same quantities for simulations performed in octane. The latter solvent is neither a donor nor an acceptor of Hbonds. Therefore, the observed exchange of peptide–solvent (red line) for peptide–peptide (black line) Hbonds in water (Fig. 3a) does not take place in octane. Without being able to form Hbonds with octane, peptides interact more with each other by forming significantly more intra-peptide (cyan line) Hbonds, which, in contrast to simulations performed in water, dominate over inter-peptide (magenta line) Hbonds for all peptide sequences studied here (Fig. 3b and Fig. S7).

Fig. 3c investigates how peptide–peptide Hbonds are formed by decomposing this quantity into contributions from backbone–backbone, backbone–sidechain, and sidechain–sidechain interactions. First, we find that the total number of peptide–peptide Hbonds (black bars) in octane is larger than that in water. This is because, in octane, Hbond donor and acceptor groups of the peptide can only be passivated by interactions with other peptide atoms, whereas, in water, they can also be passivated by interacting with the solvent. Second, Fig. 3c shows that, in water, Hbonds are formed mostly between two sidechain moieties (yellow bars) or between two backbone groups (purple bars) with only a small number of cross backbone–sidechain (red bars) interactions. In contrast, cross backbone–sidechain Hbonds are formed in large numbers in octane, which is inconsistent with the formation of secondary structures, such as α-helices or β-sheets (see Table S1).

In summary, the picture that emerges from our simulations is that, independently of the amino acid sequence, peptides F1 to F4 aggregate in polar (water) and nonpolar (octane) solvents, forming stable clusters. In octane, this is driven by the need to minimize exposure of the peptide's charged moieties to the solvent, leading to their burial in the interior of the aggregates, where they form a large number of peptide–peptide Hbonds. The latter involves simultaneously sidechain and backbone atoms of mostly the same peptide, which does not allow for the formation of secondary structures (see Fig. 4b). Accordingly, DSSP analysis (Table S2) shows that peptides in octane remain largely disordered despite the high number of hydrogen bonds. In water, charged

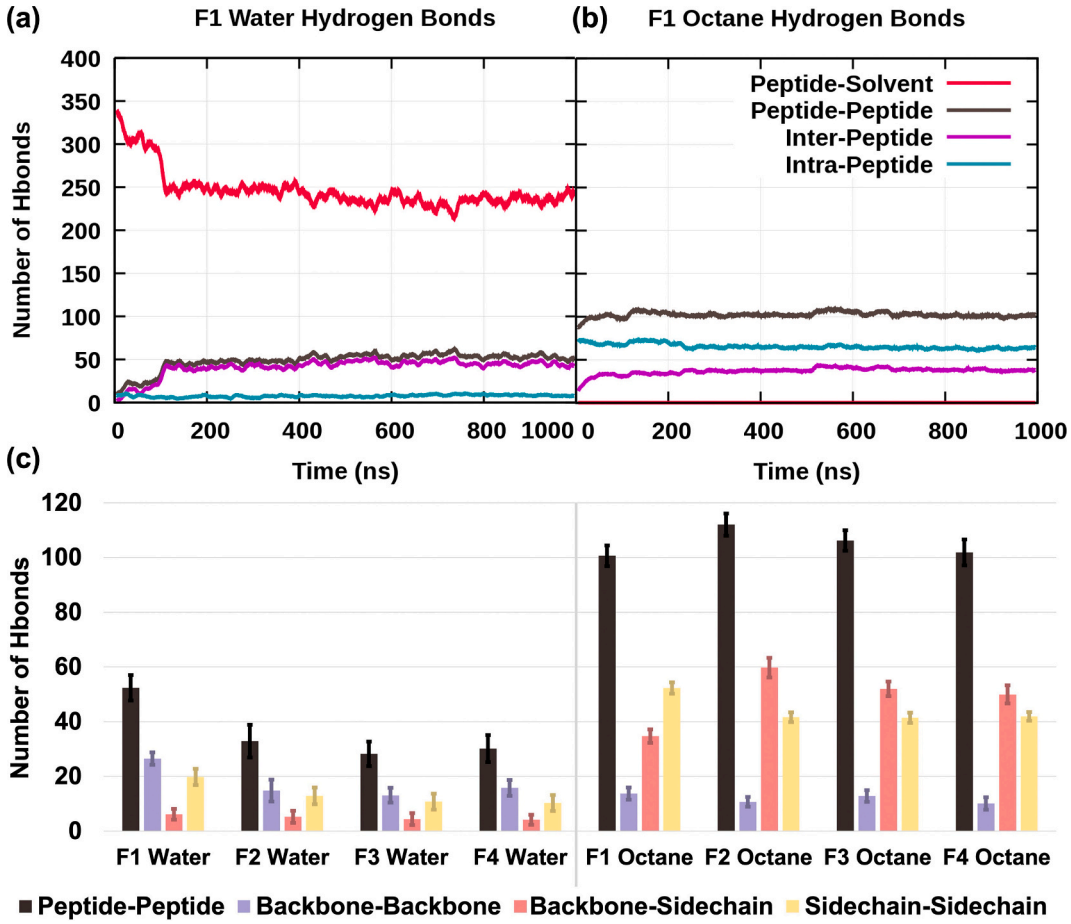

Fig. 3. Hydrogen bond analysis of peptides in different environments. The number of hydrogen bonds formed between F1 peptides (a) in water and (b) in octane. Peptide–solvent, peptide–peptide, inter-peptide, and intra-peptide hydrogen bonds are represented by red, black, magenta, and cyan, respectively. (c) The average number of peptide–peptide (black) hydrogen bonds over the last 100 ns of simulations, categorized as backbone–backbone (purple), backbone–sidechain (red), and sidechain–sidechain (yellow), averaged across all peptide sequences. Error bars indicate standard deviations. (For interpretation of the references to colour in this figure legend, the reader is referred to the web version of this article.)

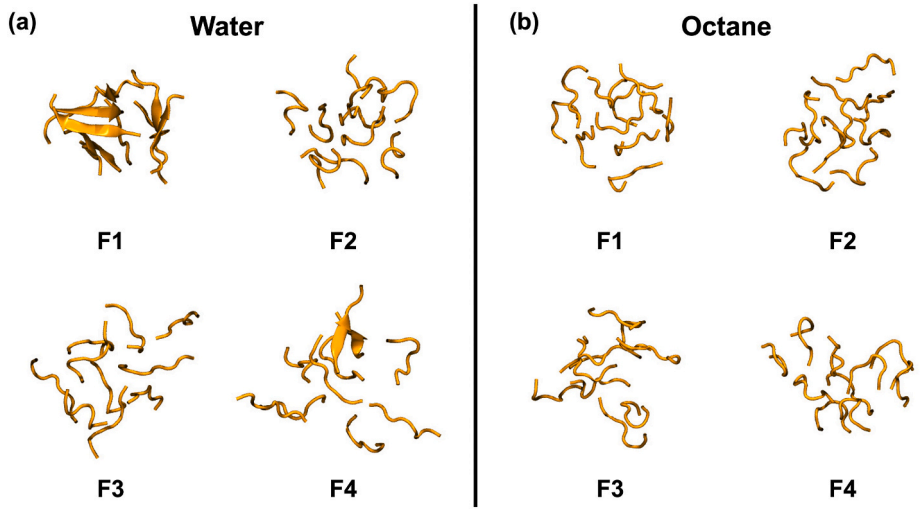

Fig. 4. Snapshots of the final configurations for all peptide sequences in (a) pure water and (b) pure octane.

sidechains interact favorably with the solvent, while nonpolar sidechains interact less with water. This leads to a partitioning of polar and nonpolar residues at the peptide–water interface, with backbone atoms positioned between these groups. As a result, Hbonds are primarily formed between sidechain–sidechain and backbone–backbone groups, with a dominant contribution from inter-peptide interactions, while backbone–sidechain interactions play a minor role. This hydrogen bonding pattern supports the formation of ordered secondary structures. Consistently, DSSP analysis (Table S2 and Fig. S3) shows that secondary structure formation is sequence dependent. In pure water, F1 exhibits the highest β-sheet structure and F2 preferentially forms α-helices. On the other hands, F3 and F4 remain largely disordered with only minor secondary structure formation. These aggregation behaviors are qualitatively supported by visualizations (Fig. 4a). The strong β-sheet propensity observed for F1 is consistent with previous experimental and computational studies showing that FKFEFKFE peptides self-assemble into β-sheet-rich structures [32,33,71].

3.3. Solvation free energy of peptides in the bulk solvent

The F1 peptide was selected as a representative sequence to investigate how the solvent environment affects solvation free energy. Table 2 summarizes the solvation free energies in pure water and pure octane solutions. The difference in solvation free energy between water and octane ($\Delta G_{Water\rightarrow Octane} = G_{Octane} - G_{Water}$) for both the monomer in its random-coil conformation and the dimer is positive, indicating that water stabilizes both peptide conformations more effectively than the nonpolar solvent. Notably, the energy difference for two monomers ($2 \times \Delta G_{Water\rightarrow Octane} = 442.70$ kJ/mol) is larger than that for the dimer (432.64 kJ/mol), suggesting that dimerization reduces residue exposure to solvent. In both solvents, the solvation free energy change associated with forming a dimer from two monomers is negative, indicating that peptide aggregation is thermodynamically favorable. In addition, the more negative dimerization free energy ($\Delta G^{2Monomer\rightarrow Dimer} = G^{Dimer} - 2 \times G^{Monomer}$) in octane (−174.20 kJ/mol) compared with water (−164.14 kJ/mol) indicates enhanced stabilization of peptide aggregation in the hydrophobic environment. This thermodynamic trend is consistent with Fig. 1a, which shows that stable aggregation is observed in octane, whereas aggregation in water displays greater fluctuations over time.

Table 2
Solvation free energies of F1 peptides in monomeric and dimeric conformations in pure water (G_{Water}), in pure octane (G_{Octane}) and the difference between solvents shown as $\Delta G_{Water\rightarrow Octane}$.

Peptide Conformation	Solvation Free Energy (kJ/mol)		
	G_{Water}	G_{Octane}	$\Delta G_{Water\rightarrow Octane}$
Monomer	−610.63 ± 38.00	−389.28 ± 39.85	221.35 ± 44.66
Dimer	−1,385.40 ± 64.85	−952.76 ± 57.22	432.64 ± 71.47

3.4. Self-assembly at the water–octane interface

Amphipathic peptides are favorably attracted to polar–nonpolar interfaces due to their composition of both hydrophobic and hydrophilic amino acids. This includes air–water [14,22,72,73] and lipid–water interfaces [21,22,28,29,74] as well as interfaces created by hydrophobic–hydrophilic solvents. At these interfaces, amphipathic peptides can aggregate and form oligomeric structures that can damage lipid membranes [15,20,24–27]. These interfacial environments are important for understanding peptide adsorption, self-assembly, and aggregation behavior. To provide insights into these interfacial effects, we study the aggregation of peptides F1 to F4 at the sharp interface of a water–octane biphasic system (Fig. 5). This interfacial environment imposes unique constraints on peptide mobility, restricting their motion to a two-dimensional plane [28], which accounts for a distinct aggregation behavior that significantly differs from what is observed in homogeneous solvents.

Amino acid partitioning at the water–octane interface is quantified in Fig. 6 by computing the coordination numbers between residues and solvent molecules in F1 peptide simulations. Given that the surface area of an octane molecule is approximately eight times larger than that of a water molecule, the coordination numbers in water are geometrically expected to be significantly higher. However, the coordination numbers of phenylalanine with water and octane are remarkably similar. This deviation from geometric expectations indicates that this nonpolar amino acid has a strong preference for the octane phase. Conversely, lysine and glutamic acid (charged amino acids) show negligible interaction with octane (coordination number ≈ 0), but strong interactions with water. This preferential exposure of charged residues to water is observed for all peptides (Fig. S8) and is consistent with results from simulations in pure water and pure octane (Fig. S6). Due to their flexibility, peptides can change their conformation and alignment to optimize the partitioning of charged and nonpolar residues at the water–octane interface. Fig. 7a shows the angle distribution between each peptide (vector connecting the first and last Cα atoms) and the z-

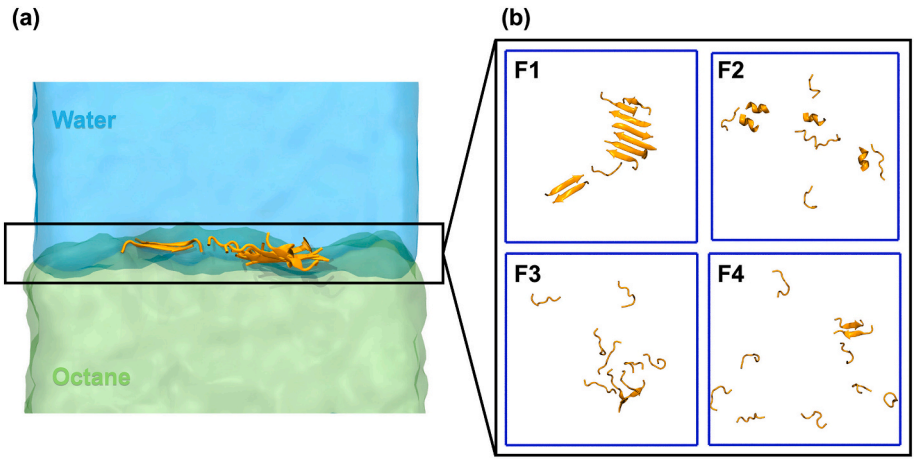

Fig. 5. (a) Side-view snapshot of the F1 peptide and (b) top-view snapshot of all peptide sequences in the final simulation frame for the water–octane system, showing peptides of all sequences localized at the interface. Peptides are shown in orange, the water phase in blue, and the octane phase in green. (For interpretation of the references to colour in this figure legend, the reader is referred to the web version of this article.)

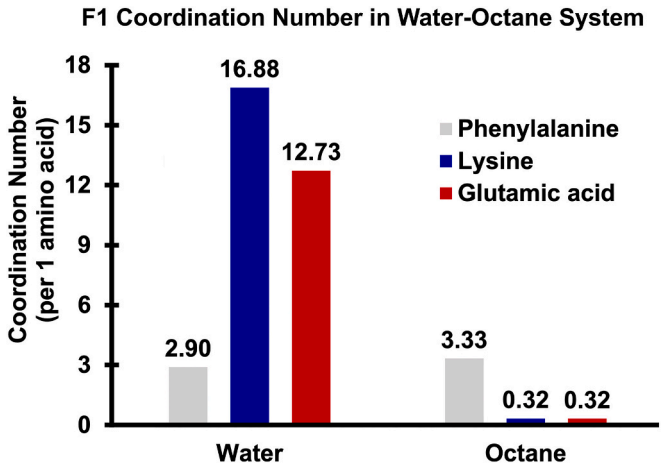

Fig. 6. Coordination number within the first coordination shell for each residue type in the F1 peptide at the water–octane interface, shown separately for residue–water and residue–octane interactions: phenylalanine (gray), lysine (blue), and glutamic acid (red). (For interpretation of the references to colour in this figure legend, the reader is referred to the web version of this article.)

axis (direction perpendicular to the interface) to quantify the structural changes. The most probable angles for peptides F1, F2, F3, and F4 are ~85°, 70°, 67°, and 59°, respectively. This indicates that the F1 peptide tends to align nearly parallel to the interface, but the F4 peptide adopts perpendicular orientations. The width of the angular distributions (Table S3) further illustrates their behavior. F1 peptides adopt a highly ordered and restricted orientation, whereas F4 peptides show the broadest distribution, indicating greater conformational flexibility. F2 and F3 sequences show intermediate characteristics in both their orientation angles and distribution widths. The most constrained orientation occurs when the segregation line separating polar and nonpolar residues (yellow line in Fig. 7b) aligns parallel to the interface, an arrangement that minimizes unfavorable solvent exposure. This result is consistent with the orientation of F1, F2, F3, and F4 peptides and the segregation of polar and nonpolar residues at the water–lipid membrane interface [24]. Peptides with narrow angular distributions and parallel orientations at the interface (e.g., F1) adopt highly ordered arrangements and promote backbone alignment between neighboring peptides. This alignment facilitates the formation of inter-peptide backbone hydrogen bonds, supporting β-sheet formation as observed in amyloid assemblies [75,76]. The interpretation is consistent with the high β-sheet content for F1 in Table S2. In contrast, peptides with broad angular distributions adopt less ordered arrangements and disrupt backbone alignment between neighboring peptides. These behaviors decrease the formation of inter-peptide backbone hydrogen bonds and cause the low β-sheet content for F4 in Table S2. These results show the important role of sequence pattern in governing peptide orientation and subsequent β-sheet formation at the interface. This orientation-dependent backbone alignment highlights the role of interfacial environments in influencing peptide organization and secondary structure formation.

3.5. *Peptide conformations and secondary structure formation at the water–octane interface*

The sequence-specific placement of nonpolar and charged residues significantly influences both peptide conformation and secondary structure formation at the water–octane interface. Fig. 8 presents the distributions of the radius of gyration (Rg) and end-to-end distance (D_{NN}). For F1 peptides (Fig. 8a), the lowest free energy is observed at high values of both Rg and D_{NN}, indicating the extended conformations of β-strand structures. This behavior has also been observed for amyloid-β on lipid membranes. The amyloid-β protein adopts extended conformations that promote β-sheet formation more effectively than the compact conformations observed on the membrane [77]. F3 and F4 peptides (Figs. 8c and 8d) are also distributed around high Rg and D_{NN} values, but their broader distributions compared with F1 suggest that their extended structures are less stable, with small β-strand propensity (see Fig. 9a) and a high likelihood of adopting compact structures.

In contrast, F2 peptides (Fig. 8b) exhibit a multimodal distribution with three distinct regions corresponding to α-helical, compact coil, and stretched coil conformations. The global free energy minimum for F2 peptides aligns with the α-helical region, indicating a strong preference for α-helix formation—unlike the other sequences. Consistently, α-helices are only observed in F2 peptides (Fig. 9b), while F1, F3, and F4 peptides favor β-strands or disordered conformations. This trend is consistent with membrane studies reporting high β-sheet propensity for F1 and α-helical propensity for F2 [24,78]. Notably, the conformational landscapes at the water–octane interface differ significantly from those in bulk solvents. In octane, the lowest free-energy states correspond to compact peptide conformations (Table S4). The nonpolar environment drives this compaction by enhancing peptide–peptide interactions. In contrast, peptides in water favor more extended conformations, except for F2 peptides, because they can form hydrogen bonds with surrounding water molecules, which stabilize the open structures and

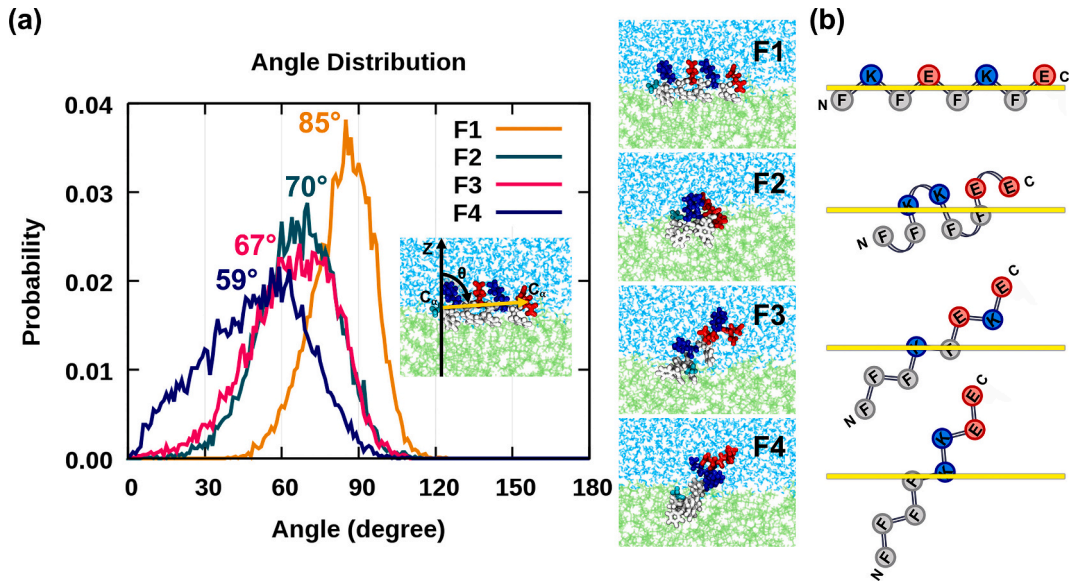

Fig. 7. Molecular characteristics of peptides at the water–octane interface. (a) Angular distribution of all peptide sequences: F1 (yellow), F2 (green), F3 (pink), and F4 (blue). Side-view snapshots show representative peptide configurations with the water and octane phases displayed in blue and green, respectively. Phenylalanine, lysine, and glutamic acid residues are colored white, blue, and red. (b) Distribution of amino acid residues in a peptide sequence. Each circle represents a specific residue: phenylalanine (F) in gray, lysine (K) in blue, and glutamic acid (E) in red. The yellow line indicates the segregation between polar and nonpolar residues. (For interpretation of the references to colour in this figure legend, the reader is referred to the web version of this article.)

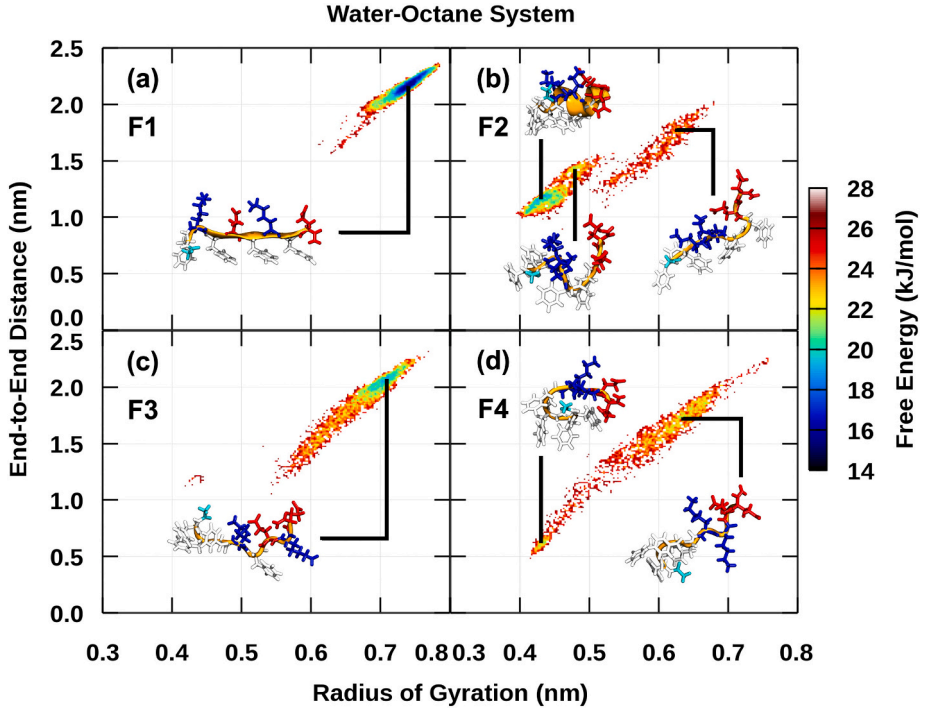

Fig. 8. Free energy landscape as a function of radius of gyration and end-to-end distance for each peptide sequence in the water–octane system: (a) F1, (b) F2, (c) F3, and (d) F4. The colour scale represents free energy (kJ/mol). Sampled structures are also provided, with phenylalanine, lysine, and glutamic acid shown in white, blue, and red, respectively. (For interpretation of the references to colour in this figure legend, the reader is referred to the web version of this article.)

results in a broader range of Rg and D_{NN} values (Fig. S9). At the interface, competing interactions from both phases further reorganize the peptides, producing conformational states that are similar to those observed in bulk water but more restricted. These findings suggest that the interface imposes spatial constraints limiting conformational diversity and promotes well defined structural states compared to bulk solvents.

Fig. 10 shows that the percentage of secondary structure and the interaction energies between backbone atoms vary across different solvent environments. A comparison of secondary structure content—specifically β-sheets and α-helices—with backbone interaction energies (comprising van der Waals and electrostatic components) reveals a clear correlation. In octane, peptides show relatively high backbone interaction energies and form disordered structures. In contrast, peptides in water show low backbone interaction energies accompanied by partial formation of secondary structures. Interestingly,

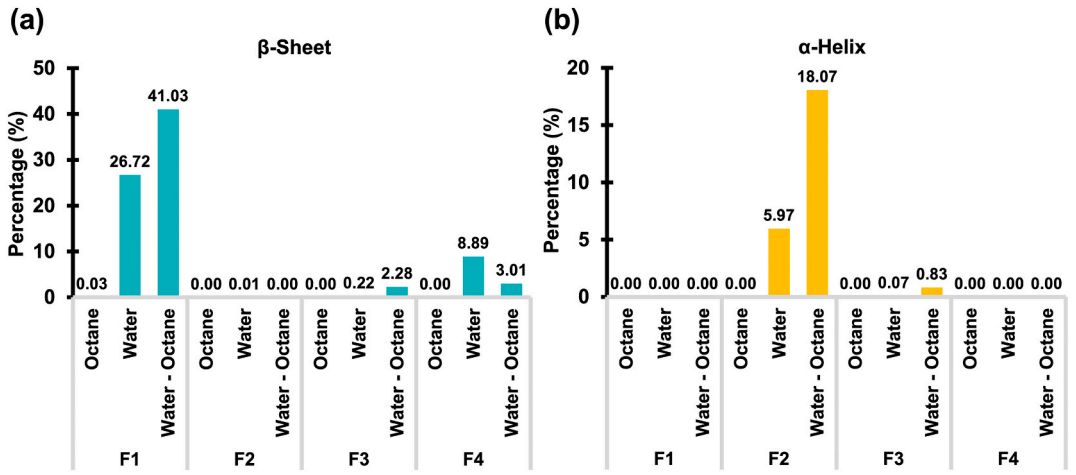

Fig. 9. Percentage distribution of peptide structures in various environments. (a) Percentage of β-sheet structures, and (b) percentage of α-helix structures.

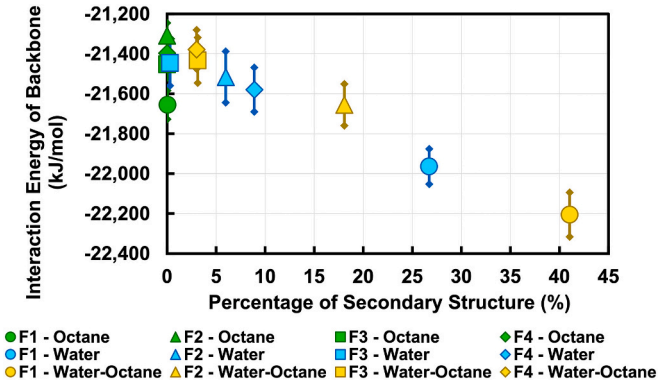

Fig. 10. Correlation between the percentage of secondary structure and backbone interaction energy of peptides F1–F4 in three different environments: octane (green), water (blue), and the water–octane interface (yellow). Each peptide is represented by a distinct marker: circles for F1, triangles for F2, squares for F3, and diamonds for F4. Error bars indicate standard deviations. (For interpretation of the references to colour in this figure legend, the reader is referred to the web version of this article.)

the water–octane interface generally shows lower backbone interaction energies and higher secondary structure contents than the bulk solvent environments. Additional time-evolution analyses of backbone interaction energy, the percentage of secondary structure, and clustering behavior are provided for the water system (Fig. S10) and the water–octane interface system (Fig. S11). The experimental and computational studies showed that Aβ42 is more efficient at aggregating in membrane environments than in bulk solution [79–82]. Although peptide behavior varies across solvent environments, F1 consistently shows the lowest backbone interaction energy and the highest secondary structure content compared with the other sequences within each environment, highlighting the important role of its alternating polar and nonpolar residue pattern in peptide aggregation behavior.

3.6. Potential of mean force profiles

Potential of mean force (PMF) calculations in Fig. 11a reveal that all examined peptide sequences exhibit a strong preference for the water–octane interface. The PMF computed in bulk water is used as our reference, i.e., PMF(water) = 0 kJ/mol. Despite being made of the same eight amino acids, the transfer free energy from bulk water to bulk octane, i.e., $\Delta PMF^{transfer} = PMF(octane) - PMF(water)$, is different for the four peptides. The value is large for sequences with segregated charged and nonpolar residues and small for sequences with alternating residue patterns because the order and type of amino acids determine

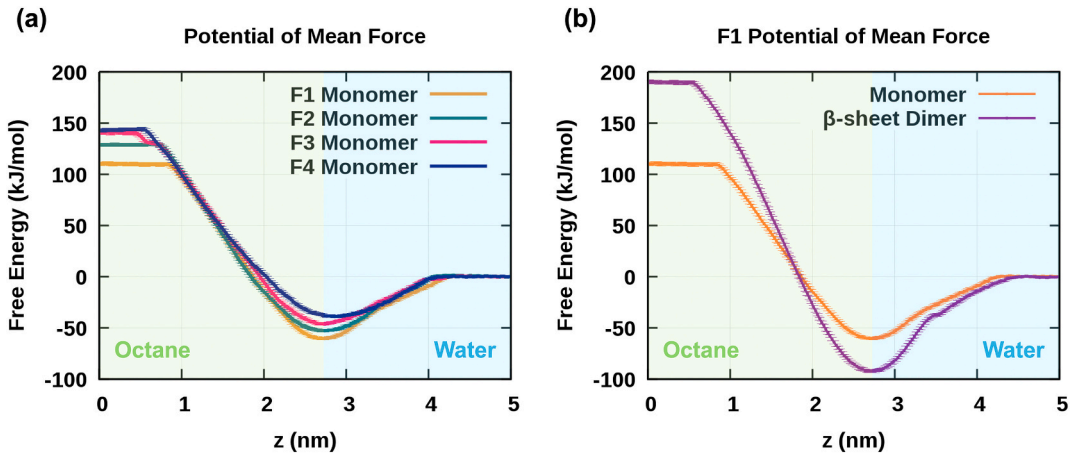

Fig. 11. PMF profiles of peptides moving across the interface from water to octane phases. (a) Comparison of PMF profiles for single peptides in random coil conformations for each peptide sequence, with F1, F2, F3, and F4 peptides represented by orange, green, pink, and blue, respectively. (b) PMF profiles for the F1 peptide, showing the monomeric peptide in orange and the β-sheet peptide dimer in purple. Error bars represent bootstrap standard deviations. The error in all systems is less than 2 kJ/mol. (For interpretation of the references to colour in this figure legend, the reader is referred to the web version of this article.)

intramolecular and peptide–solvent interactions, leading to sequence-dependent free energy profiles. Among all sequences, F1 (orange line) and F4 (blue line) peptides show the strongest and weakest preference for the interface, as they exhibit the lowest and highest free energy values at the interface. This is consistent with the broad angular distribution observed for F4 peptides in Fig. 7a, which reflects increased peptide flexibility at the interface.

Fig. 11b compares the PMF profiles of an F1 monomer in a coil configuration and an antiparallel β-sheet dimer. For the F1 peptide, the dimer PMF was calculated for a representative β-sheet-associated state to examine how peptide association in a β-sheet configuration influences transfer across the water–octane interface. Therefore, the resulting PMF describes the transfer behavior of this specific conformation. Both configurations preferentially localize at the water–octane interface. The free energy required to transfer the β-sheet dimer from bulk water to bulk octane is smaller than that required for two monomers, i.e., $\Delta PMF^{transfer}(\beta-sheet\ dimers) < 2\times\ \Delta PMF^{transfer}(monomers)$. This indicates that the peptide association in the specific β-sheet conformation reduces the energetic cost of transferring two monomers to octane. This reduction can be attributed to increased peptide–peptide interactions, which decrease the number of peptide atoms exposed to the solvent. Conversely, two monomers exhibit a stronger preference for the interface than the β-sheet dimer, i.e., $\Delta PMF^{water\rightarrow interface}(\beta-sheet\ dimers) > 2\times\ \Delta PMF^{water\rightarrow interface}(monomers)$. At the interface, charged and nonpolar residues are favorably partitioned to the water and octane phases, respectively, but exposure of these residues to the solvent is reduced for β-sheet dimers compared to monomers. For F2–F4 peptides, the dimer state is not consistently maintained along the reaction coordinate, with dissociated configurations observed in several umbrella sampling windows, particularly in the water environment. The corresponding dimer fractions for all peptides are shown in Fig. S12. Therefore, PMF calculations were not performed for F2–F4 dimers due to the instability of the dimer state.

4. Conclusion

This study used all-atom molecular dynamics simulations to investigate the role of amino acid sequence patterns on peptide aggregation across distinct environments of pure water, pure octane, and water–octane interface. Four peptides with identical compositions (4 phenylalanine, 2 lysine, and 2 glutamic acid residues) but different sequence arrangements (F1: FKFEFKFE, F2: FFKKFFEE, F3: FFFKFEKE, F4: FFFFKKEE) were systematically compared to reveal how residue ordering influences aggregation and secondary structure formation. In summary, our simulations show that:

- The hydrophobic environment of octane induced the prompt formation of a single stable cluster wherein the solvation free energy favored dimer formation over separated monomers. Charged sidechains were found enclosed within these clusters, minimizing their unfavorable interaction with the nonpolar solvent. Numerous backbone–sidechain hydrogen bonds were formed in these clusters at the expense of backbone–backbone hydrogen bonds, which impeded the formation of secondary structures in octane.
- In water, single clusters were also formed, but with nonpolar phenylalanine residues enclosed in the interior of the aggregates and charged residues exposed to the solvent. Accordingly, polar backbone atoms were left to form hydrogen bonds with other backbone atoms, enabling the formation of secondary structures: β-sheets for F1, F3, and F4 peptides, and α-helices for F2.
- At the water–octane interface, peptides exhibited a behavior that is distinct from the one observed in bulk solvents. They were found to localize preferentially at the interface, orienting nonpolar sidechains to the octane phase and polar/charged sidechains to the water phase. This partitioning of polar and nonpolar residues restricted the diffusion of peptides to the two-dimensional plane of the interface. The F1 peptide (FKFEFKFE) showed the highest interfacial ordering and rigidity, characterized by a more parallel alignment with the interface, with the other sequences displaying the broad orientational distributions. Moreover, peptides at the interface exhibited low backbone interaction energies together with high secondary structure formation, which both properties varied across different sequence patterns.

Potentials of mean force (PMF) were also computed to rationalize results from all-atom simulations. These calculations revealed that the transfer of amphipathic peptides from water to octane is highly unfavorable. This behavior is more pronounced in sequences where polar and nonpolar residues are segregated from each other as opposed to alternating within the chain. In addition, the β-sheet dimer formed by the alternating non-polar and charged residues (F1) exhibits a smaller transfer free-energy difference from water to octane than two monomers. In contrast, the favorable adsorption of peptides from water to the water–octane interface emerges as nonpolar and polar/charged sidechains partition to octane and water phases, respectively. This partitioning is highly pronounced for monomers, which possess high conformational flexibility and can readily reorient to optimize amphiphilic interactions. On the other hand, the β-sheet dimer is constrained by the inter-peptide backbone hydrogen bonds to reduce the solvent exposure at the interface. These findings provide molecular-level insight into how amphiphilic interfaces influence the adsorption, aggregation, and organization of amphipathic peptides.

Despite the insights provided by this study, it is important to also highlight its limitations. First, the model peptides used in this study were carefully selected to allow for aggregation within a few microseconds, which is the timescale accessible to computer simulations [17,83,84]. They are short (8 residues) and have an amino acid composition that is highly simplified, i.e., made of only three amino acids. This contrasts with the ~40 residues of many amyloid peptides that are made of a large number of different amino acids. However, these model peptides retain key features relevant to amyloid formation, such as amphipathic character and the ability to form similar cross-β structures [6,82]. In this context, the simplified design enables the isolation of key physicochemical interactions, such as backbone hydrogen bonding, hydrophobic association, and sequence patterning effects, which are central to amyloid aggregation but difficult to disentangle in full-length proteins. Second, our study uses a simplified water–octane interface as a minimal amphiphilic model to investigate peptide behavior at hydrophilic–hydrophobic boundaries. Similar to biological membranes, the water–octane interface contains distinct hydrophilic and hydrophobic regions that can promote peptide adsorption at interfaces. However, biological membranes are considerably complex and contain additional features such as lipid headgroups, membrane charge, and diverse lipid compositions, which influence peptide adsorption, insertion, and aggregation pathways [77,85–90]. In addition, biological membranes exhibit fluidity and bilayer asymmetry, which are not captured in the present model. In contrast, the water–octane interface provides a well-defined hydrophobic–hydrophilic boundary [28,29] that allows fundamental interfacial effects, such as peptide adsorption, hydrophobic partitioning, and sequence-dependent structural organization, to be examined in a controlled manner. Third, the simulations were performed at a temperature of 350 K, higher than physiological temperature. Elevated temperature may influence aggregation kinetics and the relative populations of secondary structures. Previous work on several amphipathic peptides has shown that aggregation occurs slowly at low temperatures, requiring substantially long simulations to observe comparable aggregation behavior [17]. Additional simulations performed at 310 K showed that the overall peptides behaviors remained qualitatively similar to those observed at 350 K. Therefore, the findings presented here are intended primarily to provide mechanistic insights into sequence- and solvent-dependent aggregation behavior rather than

peptide behavior under physiological conditions. These insights highlight how subtle variations in amino acid sequence can dramatically alter peptide self-assembly, structural preferences, and interfacial behavior. Our results also contribute to understanding the interplay between sequence pattern, solvent environment, and interfacial behavior in influencing peptide aggregation and conformational behavior.

CRediT authorship contribution statement

Siwaporn Sungted: Writing – original draft, Visualization, Methodology, Formal analysis, Data curation. **Warin Rangubpit:** Writing – review & editing, Methodology, Formal analysis, Data curation. **Saree Phongphanphanee:** Writing – review & editing, Software, Methodology. **Norio Yoshida:** Writing – review & editing, Software, Methodology. **Cristiano L. Dias:** Writing – review & editing, Visualization, Validation, Supervision, Investigation, Funding acquisition, Conceptualization. **Jirasak Wong-Ekkabut:** Writing – review & editing, Writing – original draft, Visualization, Validation, Supervision, Software, Resources, Project administration, Methodology, Investigation, Funding acquisition, Conceptualization.

Declaration of competing interest

The authors declare that they have no known competing financial interests or personal relationships that could have appeared to influence the work reported in this paper.

Acknowledgments

This work was financially supported by the National Science Research and Innovation fund (NSRF) via the Program Management Unit for Human Resources and Institutional Development, Research and Innovation [grant number B42G670041] and Kasetsart University Research and Development Institute (KURDI) through Fundamental Fund. S.S. thanks the Development and Promotion of Science and Technology Talent Project (DPST). C.L.D. and W.R. are supported by the National Institute of General Medical Health under grant no. 2R15GM148982-02. Computational resources were provided by the Academic and Research Computing System (ARCS) at the New Jersey Institute of Technology and the NSTDA Supercomputer Center (ThaiSC).

Appendix A. Supplementary data

Supplementary data to this article can be found online at https://doi.org/10.1016/j.molliq.2026.129765.

Data availability

No data was used for the research described in the article.

References

[1] J.D. Camino, P. Gracia, N. Cremades, The role of water in the primary nucleation of protein amyloid aggregation, Biophys. Chem. 269 (2021) 106520, https://doi.org/10.1016/j.bpc.2020.106520.
[2] A.K. Srivastava, J.M. Pittman, J. Zerweck, B.S. Venkata, P.C. Moore, J. R. Sachleben, S.C. Meredith, β-Amyloid aggregation and heterogeneous nucleation, Protein Sci. 28 (2019) 1567–1581, https://doi.org/10.1002/pro.3674.
[3] M. Tolar, J. Hey, A. Power, S. Abushakra, Neurotoxic soluble amyloid oligomers drive Alzheimer's pathogenesis and represent a clinically validated target for slowing disease progression, Int. J. Mol. Sci. 22 (2021) 6355, https://doi.org/10.3390/ijms22126355.
[4] N.K. Robakis, Mechanisms of AD neurodegeneration may be independent of aβ and its derivatives, Neurobiol. Aging 32 (2011) 372–379, https://doi.org/10.1016/j.neurobiolaging.2010.05.022.
[5] X. Yang, G. Meisl, B. Frohm, E. Thulin, T.P.J. Knowles, S. Linse, On the role of sidechain size and charge in the aggregation of Aβ42 with familial mutations, Proc. Natl. Acad. Sci. U. S. A. 115 (2018) E5849–E5858, https://doi.org/10.1073/pnas.1803539115.
[6] N.R. Lee, C.J. Bowerman, B.L. Nilsson, Effects of varied sequence pattern on the self-assembly of amphipathic peptides, Biomacromolecules 14 (2013) 3267–3277, https://doi.org/10.1021/bm400876s.
[7] Y. Zhao, J. Wang, L. Deng, P. Zhou, S. Wang, Y. Wang, H. Xu, J.R. Lu, Tuning the self-assembly of short peptides via sequence variations, Langmuir 29 (2013) 13457–13464, https://doi.org/10.1021/la402441w.
[8] A. Matsui, J.-P. Bellier, T. Kanai, H. Satooka, A. Nakanishi, T. Terada, T. Ishibe, Y. Nakamura, H. Taguchi, N. Naruse, Y. Mera, The effect of ethanol on disassembly of amyloid-β1-42 pentamer revealed by atomic force microscopy and gel electrophoresis, Int. J. Mol. Sci. 23 (2022) 889, https://doi.org/10.3390/ijms23020889.
[9] A.N. Rissanou, E. Georgilis, E. Kasotakis, A. Mitraki, V. Harmandaris, Effect of solvent on the self-assembly of Dialanine and diphenylalanine peptides, J. Phys. Chem. B 117 (2013) 3962–3975, https://doi.org/10.1021/jp311795b.
[10] S. Shirazi-Fard, A. Reza Zolghadr, A. Klein, How does aggregation of doxorubicin molecules affect its solvation and membrane penetration? New J. Chem. 47 (2023) 22063–22077, https://doi.org/10.1039/D2NJ06221F.
[11] E. Smorodina, B. Kav, H. Fatafta, B. Strodel, Effects of ion type and concentration on the structure and aggregation of the amyloid peptide Aβ16–22, Proteins Struct. Funct. Bioinform. 93 (2025) 1369–1382, https://doi.org/10.1002/prot.26635.
[12] S. Gotla, S. Matysiak, Mechanistic insights into the inhibition of amyloid-β aggregation by chitosan, Phys. Chem. Chem. Phys. 25 (2023) 10113–10120, https://doi.org/10.1039/D3CP00162H.
[13] Y. Chebaro, P. Derreumaux, Targeting the early steps of Aβ16–22 protofibril disassembly by N-methylated inhibitors: a numerical study, Proteins: Struct., Funct., Bioinf. 75 (2009) 442–452, https://doi.org/10.1002/prot.22254.
[14] H. Okumura, S.G. Itoh, Molecular dynamics simulations of amyloid-β(16–22) peptide aggregation at air–water interfaces, J. Chem. Phys. 152 (2020) 095101, https://doi.org/10.1063/1.5131848.
[15] Y. Yang, H. Distaffen, S. Jalali, A.J. Nieuwkoop, B.L. Nilsson, C.L. Dias, Atomic insights into amyloid-induced membrane damage, ACS Chem. Nerosci. 13 (2022) 2766–2777, https://doi.org/10.1021/acschemneuro.2c00446.
[16] Y. Yang, C.L. Dias, Peptide–Membrane Binding: Effects of the Amino Acid Sequence, J. Phys. Chem. B 127 (2023) 912–920, https://doi.org/10.1021/acs.jpcb.2c06404.
[17] S. Jalali, Y. Yang, F. Mahmoudinobar, S.M. Singh, B.L. Nilsson, C. Dias, Using all-atom simulations in explicit solvent to study aggregation of amphipathic peptides into amyloid-like fibrils, J. Mol. Liq. 347 (2022) 118283, https://doi.org/10.1016/j.molliq.2021.118283.
[18] C.J. Bowerman, D.M. Ryan, D.A. Nissan, B.L. Nilsson, The effect of increasing hydrophobicity on the self-assembly of amphipathic β-sheet peptides, Mol. Biosyst. 5 (2009) 1058–1069, https://doi.org/10.1039/B904439F.
[19] R.J. Swanekamp, J.T.M. DiMaio, C.J. Bowerman, B.L. Nilsson, Coassembly of enantiomeric amphipathic peptides into amyloid-inspired rippled β-sheet fibrils, J. Am. Chem. Soc. 134 (2012) 5556–5559, https://doi.org/10.1021/ja301642c.
[20] Y. Liu, B. Ren, Y. Zhang, Y. Sun, Y. Chang, G. Liang, L. Xu, J. Zheng, Molecular simulation aspects of amyloid peptides at membrane interface, Biochimica et Biophysica Acta (BBA) - Biomembranes 1860 (2018) 1906–1916, https://doi.org/10.1016/j.bbamem.2018.02.004.
[21] M.P. Aliste, D.P. Tieleman, Computer simulation of partitioning of ten pentapeptides ace-WLXLL at the cyclohexane/water and phospholipid/water interfaces, BMC Biochem. 6 (2005) 30, https://doi.org/10.1186/1471-2091-6-30.
[22] A. Hung, Effects of interfaces on aggregates of peptides derived from pancreatic islet amyloid polypeptide, Mol. Simul. 42 (2016) 580–595, https://doi.org/10.1080/08927022.2015.1089990.
[23] M. Bajda, S. Filipek, Study of early stages of amyloid Aβ13-23 formation using molecular dynamics simulation in implicit environments, Comput. Biol. Chem. 56 (2015) 13–18, https://doi.org/10.1016/j.compbiolchem.2015.02.014.
[24] W. Rangubpit, S. Sungted, J. Wong-Ekkabut, H.E. Distaffen, B.L. Nilsson, C.L. Dias, Pore Formation by Amyloid-like Peptides: Effects of the Nonpolar–Polar Sequence Pattern, ACS Chemical Neuroscience 15 (2024) 3354–3362, https://doi.org/10.1021/acschemneuro.4c00333.
[25] Z. Niu, Z. Zhang, W. Zhao, J. Yang, Interactions between amyloid β peptide and lipid membranes, Biochim. Biophys. Acta Biomembr. 2018 (1860) 1663–1669, https://doi.org/10.1016/j.bbamem.2018.04.004.
[26] Y. Dai, Z. Xie, L. Liang, Pore formation mechanism of A-Beta peptide on the fluid membrane: a combined coarse-grained and all-atomic model, Molecules 27 (2022) 3924, https://doi.org/10.3390/molecules27123924.
[27] A. Drajkowska, A. Molski, Transmembrane clustering of short amyloid peptide fragments: a coarse grained molecular dynamics study, Biophys. Chem. 320–321 (2025) 107418, https://doi.org/10.1016/j.bpc.2025.107418.
[28] A. Nikolic, S. Baud, S. Rauscher, R. Pomès, Molecular mechanism of β-sheet self-organization at water-hydrophobic interfaces, Proteins: Struct., Funct., Bioinf. 79 (2011) 1–22, https://doi.org/10.1002/prot.22854.
[29] A.R. Zolghadr, M. Heydari Dokoohaki, Self-assembly of neuroprotective carbazolium based small molecules at octane/water interface: a simulation investigation, Chem. Phys. 480 (2016) 1–11, https://doi.org/10.1016/j.chemphys.2016.10.008.
[30] C.M. Dobson, Protein folding and misfolding, Nature 426 (2003) 884–890, https://doi.org/10.1038/nature02261.
[31] O.S. Makin, L.C. Serpell, Structures for amyloid fibrils, FEBS J. 272 (2005) 5950–5961, https://doi.org/10.1111/j.1742-4658.2005.05025.x.
[32] D.M. Marini, W. Hwang, D.A. Lauffenburger, S. Zhang, R.D. Kamm, Left-handed helical ribbon intermediates in the self-assembly of a β-sheet peptide, Nano Lett. 2 (2002) 295–299, https://doi.org/10.1021/nl015697g.

[33] J. Bertouille, S. Kasas, C. Martin, U. Hennecke, S. Ballet, R.G. Willaert, Fast self-assembly dynamics of a β-sheet peptide soft material, Small 19 (2023) 2206795, https://doi.org/10.1002/smll.202206795.
[34] N.R. Lee, C.J. Bowerman, B.L. Nilsson, Sequence length determinants for self-assembly of amphipathic β-sheet peptides, Biopolymers 100 (2013) 738–750, https://doi.org/10.1002/bip.22248.
[35] C.J. Bowerman, W. Liyanage, A.J. Federation, B.L. Nilsson, Tuning β-sheet peptide self-assembly and hydrogelation behavior by modification of sequence hydrophobicity and aromaticity, Biomacromolecules 12 (2011) 2735–2745, https://doi.org/10.1021/bm200510k.
[36] F. Yanchik-Slade, J. Hofe, B. Nilsson, Chirality in Peptide Self-Assembly and Aggregation, in: Pept. Bionanomaterials, 2023, pp. 229–253, https://doi.org/10.1007/978-3-031-29360-3_7.
[37] C.W. Jones, J. Chen, R. Panda, S. Jalali, L.P. Cardani, Y. Guo, I.M. Arnold, C. L. Dias, B.L. Nilsson, Comparison of pleated and rippled β-sheet assembly of sequence isomers of an amphipathic self-assembling peptide, Biochemistry 65 (2026) 994–1012, https://doi.org/10.1021/acs.biochem.6c00035.
[38] F. Wang, O. Gnewou, S. Wang, T. Osinski, X. Zuo, E.H. Egelman, V.P. Conticello, Deterministic chaos in the self-assembly of β sheet nanotubes from an amphipathic oligopeptide, Matter 4 (2021) 3217–3231, https://doi.org/10.1016/j.matt.2021.06.037.
[39] W.L. Jorgensen, J. Chandrasekhar, J.D. Madura, R.W. Impey, M.L. Klein, Comparison of simple potential functions for simulating liquid water, J. Chem. Phys. 79 (1983) 926–935, https://doi.org/10.1063/1.445869.
[40] J. Huang, S. Rauscher, G. Nawrocki, T. Ran, M. Feig, B.L. de Groot, H. Grubmüller, A.D. MacKerell, CHARMM36m: an improved force Field for folded and intrinsically disordered proteins, Nat. Methods 14 (2017) 71–73, https://doi.org/10.1038/nmeth.4067.
[41] R.B. Best, X. Zhu, J. Shim, P.E.M. Lopes, J. Mittal, M. Feig, A.D. Jr, MacKerell, optimization of the additive CHARMM all-atom protein force Field targeting improved sampling of the backbone φ, ψ and side-chain χ1 and χ2 dihedral angles, J. Chem. Theory Comput. 8 (2012) 3257–3273, https://doi.org/10.1021/ct300400x.
[42] A.D. Mackerell, M. Feig, C.L. Brooks, Extending the treatment of backbone energetics in protein force fields: limitations of gas-phase quantum mechanics in reproducing protein conformational distributions in molecular dynamics simulations, J. Comput. Chem. 25 (2004) 1400–1415, https://doi.org/10.1002/jcc.20065.
[43] A.D. MacKerell, D. Bashford, M. Bellott, R.L. Dunbrack, J.D. Evanseck, M.J. Field, S. Fischer, J. Gao, H. Guo, S. Ha, D. Joseph-McCarthy, L. Kuchnir, K. Kuczera, F.T. K. Lau, C. Mattos, S. Michnick, T. Ngo, D.T. Nguyen, B. Prodhom, W.E. Reiher, B. Roux, M. Schlenkrich, J.C. Smith, R. Stote, J. Straub, M. Watanabe, J. Wiórkiewicz-Kuczera, D. Yin, M. Karplus, All-Atom Empirical Potential for Molecular Modeling and Dynamics Studies of Proteins, J. Phys. Chem. B 102 (1998) 3586–3616, https://doi.org/10.1021/jp973084f.
[44] M.J. Abraham, T. Murtola, R. Schulz, S. Páll, J.C. Smith, B. Hess, E. Lindahl, GROMACS: high performance molecular simulations through multi-level parallelism from laptops to supercomputers, SoftwareX 1 (2) (2015) 19–25, https://doi.org/10.1016/j.softx.2015.06.001.
[45] T. Darden, D. York, L. Pedersen, Particle mesh Ewald: an N·log(N) method for Ewald sums in large systems, J. Chem. Phys. 98 (1993) 10089–10092, https://doi.org/10.1063/1.464397.
[46] U. Essmann, L. Perera, M.L. Berkowitz, T. Darden, H. Lee, L.G. Pedersen, A smooth particle mesh Ewald method, J. Chem. Phys. 103 (1995) 8577–8593, https://doi.org/10.1063/1.470117.
[47] B. Hess, P-LINCS: a parallel linear constraint solver for molecular simulation, J. Chem. Theory Comput. 4 (2008) 116–122, https://doi.org/10.1021/ct700200b.
[48] G. Bussi, D. Donadio, M. Parrinello, Canonical sampling through velocity rescaling, J. Chem. Phys. 126 (2007) 014101, https://doi.org/10.1063/1.2408420.
[49] M. Parrinello, A. Rahman, Polymorphic transitions in single crystals: a new molecular dynamics method, J. Appl. Phys. 52 (1981) 7182–7190, https://doi.org/10.1063/1.328693.
[50] W. Humphrey, A. Dalke, K. Schulten, VMD: visual molecular dynamics, J. Mol. Graph. 14 (1996) 33–38, https://doi.org/10.1016/0263-7855(96)00018-5.
[51] E. Ermakova, O. Makshakova, R. Kurbanov, I. Ibraev, Y. Zuev, I. Sedov, Aggregation of amyloidogenic peptide Uperin—molecular dynamics simulations, Molecules 28 (2023) 4070, https://doi.org/10.3390/molecules28104070.
[52] B. Khurshid, A.U. Rehman, R. Luo, A. Khan, A. Wadood, J. Anwar, Heparin-assisted Amyloidogenesis uncovered through molecular dynamics simulations, ACS Omega 7 (2022) 15132–15144, https://doi.org/10.1021/acsomega.2c01034.
[53] S. Horowitz, R.C. Trievel, Carbon-oxygen hydrogen bonding in biological structure and function, J. Biol. Chem. 287 (2012) 41576–41582, https://doi.org/10.1074/jbc.R112.418574.
[54] W. Kabsch, C. Sander, Dictionary of protein secondary structure: pattern recognition of hydrogen-bonded and geometrical features, Biopolymers 22 (1983) 2577–2637, https://doi.org/10.1002/bip.360221211.
[55] Y. Yu, J.B. Klauda, Update of the CHARMM36 united atom chain model for hydrocarbons and phospholipids, J. Phys. Chem. B 124 (2020) 6797–6812, https://doi.org/10.1021/acs.jpcb.0c04795.
[56] W. Huang, N. Blinov, A. Kovalenko, Octanol–Water Partition Coefficient from 3D-RISM-KH Molecular Theory of Solvation with Partial Molar Volume Correction, J. Phys. Chem. B 119 (2015) 5588–5597, https://doi.org/10.1021/acs.jpcb.5b01291.
[57] D. Roy, N. Blinov, A. Kovalenko, Predicting accurate solvation free energy in n-octanol using 3D-RISM-KH molecular theory of solvation: making right choices, J. Phys. Chem. B 121 (2017) 9268–9273, https://doi.org/10.1021/acs.jpcb.7b06375.
[58] T. Luchko, N. Blinov, G.C. Limon, K.P. Joyce, A. Kovalenko, SAMPL5: 3D-RISM partition coefficient calculations with partial molar volume corrections and solute conformational sampling, J. Comput. Aided Mol. Des. 30 (2016) 1115–1127, https://doi.org/10.1007/s10822-016-9947-7.
[59] N. Tielker, D. Tomazic, L. Eberlein, S. Güssregen, S.M. Kast, The SAMPL6 challenge on predicting octanol–water partition coefficients from EC-RISM theory, J. Comput. Aided Mol. Des. 34 (2020) 453–461, https://doi.org/10.1007/s10822-020-00283-4.
[60] F. Hirata, Molecular Theory of Solvation, Kluwer Academic, Dordrecht, 2003.
[61] Y. Maruyama, N. Yoshida, RISMiCal: a software package to perform fast RISM/3D-RISM calculations, J. Comput. Chem. 45 (2024) 1470–1482, https://doi.org/10.1002/jcc.27340.
[62] N. Yoshida, The reference interaction site model integrated calculator (RISMiCal) program package for nano- and biomaterials design, IOP Conf. Ser. Mater. Sci. Eng. 773 (2020) 012062, https://doi.org/10.1088/1757-899X/773/1/012062.
[63] S. Kumar, J.M. Rosenberg, D. Bouzida, R.H. Swendsen, P.A. Kollman, THE weighted histogram analysis method for free-energy calculations on biomolecules. I. THE method, J. Comput. Chem. 13 (1992) 1011–1021, https://doi.org/10.1002/jcc.540130812.
[64] J.S. Hub, B.L. de Groot, D. van der Spoel, g_wham—a free weighted histogram analysis implementation including robust error and autocorrelation estimates, J. Chem. Theory Comput. 6 (2010) 3713–3720, https://doi.org/10.1021/ct100494z.
[65] B. Kav, B. Strodel, Does the inclusion of electronic polarisability lead to a better modelling of peptide aggregation? RSC Adv. 12 (2022) 20829–20837, https://doi.org/10.1039/D2RA01478E.
[66] J. Hjalte, S. Hossain, A. Hugerth, H. Sjögren, M. Wahlgren, P. Larsson, D. Lundberg, Aggregation behavior of structurally similar therapeutic peptides investigated by 1H NMR and all-atom molecular dynamics simulations, Mol. Pharm. 19 (2022) 904–917, https://doi.org/10.1021/acs.molpharmaceut.1c00883.
[67] I. Khoiroh, S.Y. Lee, M. Pirdashti, M.-J. Lee, Insight into structural properties of polyethylene glycol monolaurate in water and alcohols from molecular dynamics studies, RSC Adv. 10 (2020) 21760–21771, https://doi.org/10.1039/C9RA09688D.
[68] A. Iscen, K. Kaygisiz, C.V. Synatschke, T. Weil, K. Kremer, Multiscale simulations of self-assembling peptides: surface and Core hydrophobicity determine fibril stability and amyloid aggregation, Biomacromolecules 25 (2024) 3063–3075, https://doi.org/10.1021/acs.biomac.4c00151.
[69] C. Narayanan, C.L. Dias, Hydrophobic interactions and hydrogen bonds in β-sheet formation, J. Chem. Phys. 139 (2013) 115103, https://doi.org/10.1063/1.4821596.
[70] Z. Su, C.L. Dias, Driving β-strands into fibrils, J. Phys. Chem. B 118 (2014) 10830–10836, https://doi.org/10.1021/jp504798s.
[71] S. Jalali, R. Zhang, M.P. Haataja, C.L. Dias, Nucleation and growth of amyloid fibrils, J. Phys. Chem. B 127 (2023) 9759–9770, https://doi.org/10.1021/acs.jpcb.3c05300.
[72] S.G. Itoh, M. Yagi-Utsumi, K. Kato, H. Okumura, Effects of a hydrophilic/hydrophobic Interface on amyloid-β peptides studied by molecular dynamics simulations and NMR experiments, J. Phys. Chem. B 123 (2019) 160–169, https://doi.org/10.1021/acs.jpcb.8b11609.
[73] C. Dalgicdir, C. Globisch, C. Peter, M. Sayar, Tipping the scale from disorder to alpha-helix: folding of amphiphilic peptides in the presence of macroscopic and molecular interfaces, PLoS Comput. Biol. 11 (2015) e1004328, https://doi.org/10.1371/journal.pcbi.1004328.
[74] M.P. Aliste, J.L. MacCallum, D.P. Tieleman, Molecular dynamics simulations of pentapeptides at interfaces: salt bridge and cation−π interactions, Biochemistry 42 (2003) 8976–8987, https://doi.org/10.1021/bi027001j.
[75] R. Nelson, M.R. Sawaya, M. Balbirnie, A.Ø. Madsen, C. Riekel, R. Grothe, D. Eisenberg, Structure of the cross-β spine of amyloid-like fibrils, Nature 435 (2005) 773–778, https://doi.org/10.1038/nature03680.
[76] P.C.A. van der Wel, J.R. Lewandowski, R.G. Griffin, Structural characterization of GNNQQNY amyloid fibrils by magic angle spinning NMR, Biochemistry 49 (2010) 9457–9469, https://doi.org/10.1021/bi100077x.
[77] A. Sahoo, H. Xu, S. Matysiak, Pathways of amyloid-beta absorption and aggregation in a membranous environment, Phys. Chem. Chem. Phys. 21 (2019) 8559–8568, https://doi.org/10.1039/C9CP00040B.
[78] W. Rangubpit, H.E. Distaffen, B.L. Nilsson, C.L. Dias, Insights into membrane damage by α-helical and β-sheet peptides, Biomolecules 15 (2025) 973, https://doi.org/10.3390/biom15070973.
[79] J.J. Kremer, R.M. Murphy, Kinetics of adsorption of beta-amyloid peptide Abeta(1-40) to lipid bilayers, J. Biochem. Biophys. Methods 57 (2003) 159–169, https://doi.org/10.1016/s0165-022x(03)00103-9.
[80] M. Bokvist, F. Lindström, A. Watts, G. Gröbner, Two types of Alzheimer's β-amyloid (1–40) peptide membrane interactions: aggregation preventing transmembrane anchoring *versus* accelerated surface fibril formation, J. Mol. Biol. 335 (2004) 1039–1049, https://doi.org/10.1016/j.jmb.2003.11.046.
[81] M. Bokvist, G. Gröbner, Misfolding of amyloidogenic proteins at membrane surfaces: the impact of macromolecular crowding, J. Am. Chem. Soc. 129 (2007) 14848–14849, https://doi.org/10.1021/ja076059o.
[82] S. Banerjee, M. Hashemi, K. Zagorski, Y.L. Lyubchenko, Interaction of Aβ42 with membranes triggers the self-assembly into oligomers, Int. J. Mol. Sci. 21 (2020) 1129, https://doi.org/10.3390/ijms21031129.

[83] B.L. Nilsson, G. Celebi Torabfam, C.L. Dias, Peptide self-assembly into amyloid fibrils: unbiased all-atom simulations, J. Phys. Chem. B 128 (2024) 3320–3328, https://doi.org/10.1021/acs.jpcb.3c07861.
[84] B.J. Williams-Noonan, A. Kamboukos, N. Todorova, I. Yarovsky, Self-assembling peptide biomaterials: insights from spontaneous and enhanced sampling molecular dynamics simulations, Chem. Phys. Rev. 4 (2023) 021304, https://doi.org/10.1063/5.0142302.
[85] S. Banerjee, M. Hashemi, K. Zagorski, Y.L. Lyubchenko, Cholesterol in membranes facilitates aggregation of amyloid β protein at physiologically relevant concentrations, ACS Chem. Nerosci. 12 (2021) 506–516, https://doi.org/10.1021/acschemneuro.0c00688.
[86] M. Jain, S. Matysiak, Dual role of anionic lipids in amyloid aggregation, J. Phys. Chem. B 128 (2024) 10831–10840, https://doi.org/10.1021/acs.jpcb.4c05636.
[87] K. Akiho, A. Iida-Adachi, H. Nabika, Opposite roles of cholesterol and lanosterol in lipid membrane on amyloid-Beta 42 peptide nucleation and fibril formation, ACS Chem. Nerosci. 16 (2025) 195–202, https://doi.org/10.1021/acschemneuro.4c00707.
[88] Y. Yang, B. Shah, M. Agapito, A.J. Nieuwkoop, Effects of cholesterol on amyloid-induced membrane poration, 2025, https://doi.org/10.1101/2025.08.15.670631.
[89] A. Khursheed, J.H. Viles, Impact of membrane phospholipids and exosomes on the kinetics of amyloid-β fibril assembly, J. Mol. Biol. 436 (2024) 168464, https://doi.org/10.1016/j.jmb.2024.168464.
[90] E. Terzi, G. Hölzemann, J. Seelig, Interaction of Alzheimer β-amyloid peptide (1−40) with lipid membranes, Biochemistry 36 (1997) 14845–14852, https://doi.org/10.1021/bi971843e.